Hydraulic Optimization of an Adjustable Spiral-Shaped Evaporator

Matthias Feiner, Francisco Javier Fernández García, Michael Arneman, Martin Kipfmüller

***Abstract*—**To ensure reliability in miniaturized devices or processes with increased heat fluxes, very efficient cooling methods have to be employed in order to cope with small available cooling surfaces. To address this problem, a certain type of evaporator/heat exchanger was developed: It is called a swirl evaporator due to its flow characteristic. The swirl evaporator consists of a concentrically eroded screw geometry in which a capillary tube is guided, which is inserted into a pocket hole in components with high heat load. The liquid refrigerant R32 is sprayed through the capillary tube to the end face of the blind hole and is sucked off against the injection direction in the screw geometry. Its inner diameter is between one and three millimeters. The refrigerant is sprayed into the pocket hole via a small tube aligned in the center of the bore hole and is sucked off on the front side of the hole against the direction of injection. The refrigerant is sucked off in a helical geometry (twisted flow) so that it is accelerated against the hot wall (centrifugal acceleration). This results in an increase in the critical heat flux of up to 40%. In this way, more heat can be dissipated on the same surface/available installation space. This enables a wide range of technical applications. To optimize the design for the needs in various fields of industry, like the internal tool cooling when machining nickel base alloys like Inconel 718, a correlation-based model of the swirl-evaporator was developed. The model is separated into 3 subgroups with overall 5 regimes. The pressure drop and heat transfer are calculated separately. An approach to determine the locality of phase change in the capillary and the swirl was implemented. A test stand has been developed to verify the simulation.

***Keywords*—**Helically-shaped, oil-free, R32, swirl-evaporator, twist flow.

I. Introduction

SINCE the beginning of industrial production, the aim has always been to improve the performance of processes. Through efficient and process-oriented cooling, it is possible to shorten the cycle time in production lines through faster processes and thus produce more economically.

In order to save construction costs, products and its components are becoming smaller and smaller, but often retain or even increase their performance. This leads to the problem of heat generation and heat dissipation in many applications. An example for this is the increase of performance of machine tools and the resulting process heat, which has already been discussed by [14]. Here, large heat fluxes have to be dissipated in a very confined space in order to guarantee the performance increase with constant quality of the components.

Another example is the cooling of processors, which develop extremely high heat flux even in smallest spaces and are therefore limited in their overclocking. More efficient cooling with miniaturized evaporators could further increase the performance of processors without having to develop even smaller diodes in half-conductor technology. Therefore, the Institute for Materials and Processes is investigating a new evaporator form which should fulfill the above-mentioned tasks. With the model, one should be able to make statements about the pressure loss, heat transfer, critical heat flux.

In this paper the swirl evaporator is simulated by a correlation-based computer model. For this purpose, suitable correlations to the individual subprocesses occurring in the swirl evaporator must be found. The main focus of the calculation should be the determination of heat transfer of the swirl evaporator. For this purpose, it is also necessary to calculate the pressure losses that occur exactly in the swirl evaporator and are generated by the swirl for the calculation of mass flow. Therefore, the calculation of pressure losses is also an essential part of this work.

The calculated results are then validated with existing measurement data to prove the validity of the simulation program created. The resulting recommendations for the further improvement of the swirl evaporator are given at the end of the report.

The objective is to be able to carry out the complete design and scaling of the swirl evaporator with this program in order to finally obtain a marketable product which can be precisely adapted to the respective processes to be carried out.

II. Description of the Experimental Rig

As shown in Fig. 1 the swirl evaporator consists of a cylindrical bush into which a screw with an internal bore (capillary) is inserted. The refrigerant flows through the capillary and begins to evaporate due to the frictional pressure losses. At the capillary outlet, it expands as a spray channel onto the cooling wall of the bush. The counterflow, which is rotated by 180°, enters the screw-like swirl in two phases and continues to evaporate. Under certain operating conditions, overheating can occur. A detailed description of the test facility in which the experiments were performed, as well as the operating conditions and system uncertainties can be found in [10]. Fig. 1 shows the profile of the testing rig with its main parts.

Fig. 2 shows the cycle process of the refrigerant. The bold line shows the process steps which take place in the swirl evaporator itself. In the capillary tube which supplies the refrigerant to the blind hole the 1-phase (1→2) and 2-phase pressure drop (2→3) takes place. At the bottom of the blind hole the refrigerant is sprayed from the capillary tube onto the

Matthias Helmut Feiner is with the Karlsruhe University of Applied Sciences, Germany (e-mail: matthias.feiner@hs-karlsruhe.de).

hot wall. In this area of spray cooling, also called spot evaporator (3→4), the refrigerant evaporates almost isobarically. The refrigerant is then fed into the swirl part of the evaporator (4→5) where, depending on the heat load and mass flow, the refrigerant can already overheat (5→6). After this the refrigerant is discharged into the post evaporator to assure a fixed overheating for compressor safety before it

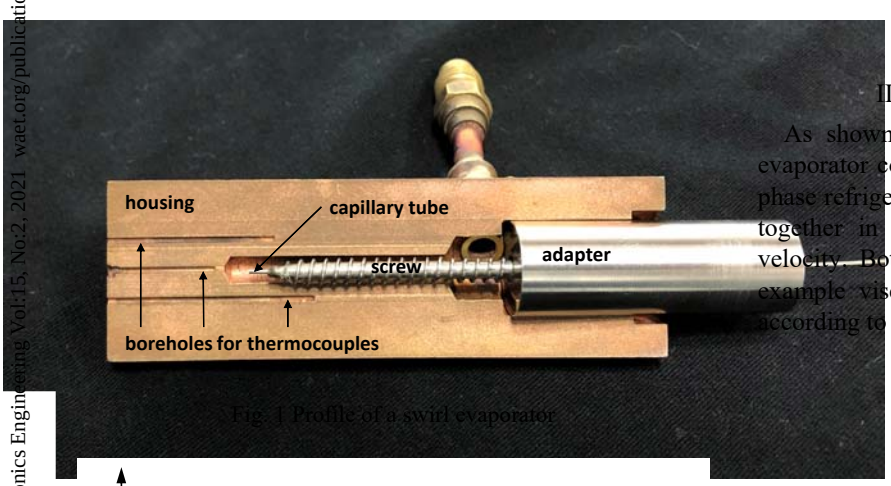

Fig. 1 Profile of a swirl evaporator

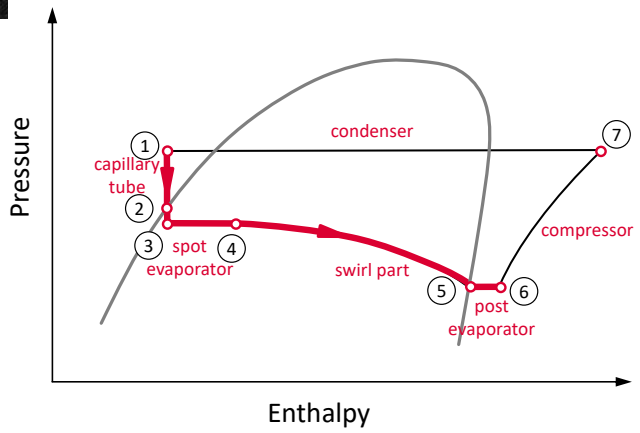

Fig. 2 Cycle process in the swirl evaporator in the p-h diagram

The swirl evaporator is modeled with the Engineering Equation Solver (EES) program and is divided into 5 regimes. Within one regime a part of the swirl evaporator can be unified, for which the thermohydraulic change of state of the flow can be quantified with the same empirical calculation model. Analytical equations are used, which are operated with a large number of parameters. The regimes are composed of the capillary with 1- and 2-phase area, the spray and swirl area again with 1-phase superheated and a 2-phase area. Fig. 3 shows the considered 3 subgroups and 5 regimes. The refrigerant enters the swirl evaporator through the capillary tube which also causes a pressure drop due to frictional losses. Depending on the pressure loss in the capillary tube (mainly a function of the hydraulic diameter, length and flow velocity) a 2-phase state can occur. After being sprayed at the hot front surface of the bore whole the refrigerant is led into the swirl where it evaporates and, should the situation arise, overheats.

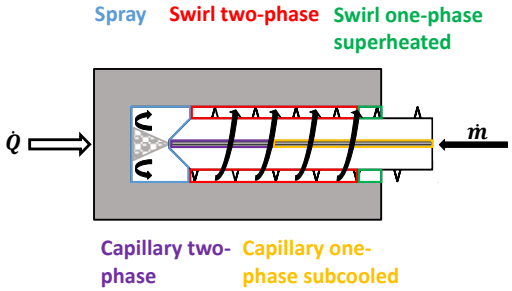

Fig. 3 Regimes of a swirl evaporator

III. Setup of the Simulation Model

As shown in Fig. 3, the simulation model of the swirl evaporator consists of 5 different regimes. In regimes with 2-phase refrigerant state, gaseous and liquid phase are described together in one model, ergo defined with the same flow velocity. Both phases have different material properties, for example viscosity. For the simulation, the viscosity model according to [1] is,

$$\nu_{tp} = \frac{\nu_L}{1 - x + x \cdot \left(\frac{\varrho_L}{\varrho_G}\right)^{0.5}} \tag{1}$$

The pressure loss of the regime is calculated as a function of the Reynolds number according to correlations from the VDI Heat Atlas [2]. For a laminar flow ergo Reynolds numbers smaller than 2320 the drag coefficient ζ are calculated according to Hagen-Poiseuille's law [11]

$$\zeta = \frac{64}{Re} \tag{2}$$

For turbulent flows and in the range of Reynolds numbers between 3000 and 100,000, (3) is used [12]:

$$\zeta = \frac{0{,}3164}{\sqrt[4]{Re}} \tag{3}$$

For the range between Reynolds numbers 10^4 and 10^6 the equation of Konakov is used [13]

$$\zeta = (1{,}8 \cdot \lg Re - 1{,}5)^{-2} \tag{4}$$

For the pressure loss 2-phase in a straight horizontal pipe, only the pressure loss due to friction is used in this application. The acceleration part is neglected due to low evaporation in the capillary. Since the flow form is unknown, the correlation of [2] is suitable.

$$\Delta p_{tp} = \frac{dL \cdot 2 \cdot \rho_M \cdot w_M^2}{D} \cdot \left(0{,}0925 \cdot Re^{-0{,}2534} + \frac{\left(13{,}98 \cdot Re^{-0{,}9501} - 0{,}0925 \cdot Re^{-0{,}2534}\right)}{\left(1 + \left(\frac{Re}{293}\right)^{4{,}864}\right)^{0{,}1972}}\right) \tag{5}$$

The mixture density is calculated according to:

$$\rho_M = \rho_L \cdot \lambda_L + \rho_G \cdot (1 - \lambda_L) \tag{6}$$

whereby the volume flow rate λ_L is determined according to

$$\lambda_L = \frac{\dot{V}_L}{\dot{V}_L + \dot{V}_G} \tag{7}$$

The mean flow velocity w_M is composed as the sum of the empty pipe gas velocity w_G and the empty pipe liquid velocity w_L.

$$w_G = \frac{\dot{V}_G}{A} = \frac{\dot{m} \cdot x}{\rho_G \cdot A} \tag{8}$$

$$w_L = \frac{\dot{V}_L}{A} = \frac{\dot{m} \cdot (1-x)}{\rho_L \cdot A} \tag{9}$$

Due to the dominant share of the liquid phase in the total pressure drop, the average Reynolds number is calculated exclusively with the viscosity for the liquid phase according to:

$$Re = \frac{w_M \cdot D \cdot \rho_L}{\eta_L} \tag{10}$$

For this regime, a correlation by Chisholm was used as presented in [3]. The model considers a 2-phase state during spraying from the capillary and the influence of the countercurrent. The model assumes an expansion due to a sudden change in cross-section up to half the bore diameter as shown in Fig. 4. The 2-phase pressure drop $\Delta p_{tp,Spray}$ consists of the product

$$\Delta p_{tp,Spray} = \Delta p_0 \cdot \gamma_{Spray} \tag{11}$$

The factors are calculated according to:

$$\gamma_{Spray} = 1 + \left(\left(\frac{v_G}{v_L}\right) - 1\right) \cdot (B \cdot x \cdot (1-x) + x^2) \tag{12}$$

$$B = \left(\frac{1}{k_{slip}}\right)^{0,28} \tag{13}$$

For $X_{xp} > 1$ gilt the following applies:

$$k_{slip} = \left(\frac{v_G}{v_L}\right)^{0,25} \tag{14}$$

Otherwise, the following applies:

$$k_{slip} = 1 + x \cdot \left(\frac{v_G}{v_L} - 1\right)^{0,5} \tag{15}$$

The size X_{xp} is calculated according to:

$$X_{xp} = \frac{1-x}{x} \cdot \left(\frac{v_L}{v_G}\right)^{0,5} \tag{16}$$

The equation applies to the 1-phase pressure drop:

$$\Delta p_0 = \frac{\zeta_{Spray} \cdot G^2 \cdot v_L}{2} \tag{17}$$

$$\zeta_{Spray} = \left(-\frac{2}{\sigma_{ar}}\right) \cdot \left(1 - \left(\frac{1}{\sigma_{ar}}\right)\right) \tag{18}$$

$$\sigma_{ar} = \frac{\left(\frac{D_{Evap}}{2}\right)^2}{d^2_{capillary}} \tag{19}$$

A correlation of [4] was used for the 2-phase range in the swirl. The equations were determined with the fluid water, at a helix tube diameter of 10 mm, a diameter ratio $D_{Evap}/D_{hyd_{Swirl}}$ between 13 and 25, pressures between 5 and 35 bar and mass flow rates between 150 and 1760 $kg/m^2 \cdot s$. Since water and R32 in liquid and gaseous state differ greatly, errors must be expected. However, since the helix geometry is well suited for this application and better alternatives were not available, this was left. Guo modified a correlation of [5] for straight pipes with experimental data for swirl flow. It is noticeable that the slope of the helix was not considered.

$$\Delta p_{tp_{Swirl}} = \Phi \cdot \Delta p_0 \tag{20}$$

for $G < 1000 \frac{kg}{m^2 \cdot s}$:

$$\Phi = 142{,}2 \cdot \psi \cdot \left(\frac{p}{p_{krit}}\right)^{0,62} \cdot \left(\frac{d}{D}\right)^{1,04} \cdot \left(1 + x \cdot \left(\frac{\rho_L}{\rho_G} - 1\right)\right) \tag{21}$$

for $G \geq 1000 \frac{kg}{m^2 \cdot s}$:

$$\psi = 1 + \frac{x \cdot (1-x) \cdot \left(\frac{1000}{G} - 1\right) \cdot \left(\frac{\rho_L}{\rho_G}\right)}{1 + x \cdot \left(\frac{\rho_L}{\rho_G} - 1\right)} \tag{22}$$

$$\psi = 1 + \frac{x \cdot (1-x) \cdot \left(\frac{1000}{G} - 1\right) \cdot \left(\frac{\rho_L}{\rho_G}\right)}{1 + (1-x) \cdot \left(\frac{\rho_L}{\rho_G} - 1\right)} \tag{23}$$

The pressure loss Δp_0 is calculated according to the correlations in chapter 6.2.2 of [2] for straight pipes. The length $l_{0,Swirl}$ of the flow path is calculated according to:

$$l_{0,Swirl} = n \cdot \pi \cdot D \tag{24}$$

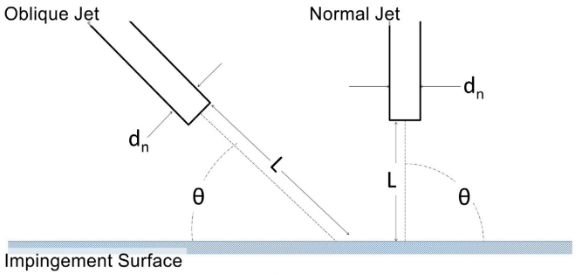

Fig. 4 Injection angle on the cooling surface [7]

The Nusselt correlation used comes from [6]. The basis is a correlation according to [7] for the fluid air. By modification, the correlation is also applicable to other unspecified fluids. The result is a correlation for the Nusselt number.

$$Nu_{\text{Spray}} = Re_{\text{d}_{\text{capillary}}}^{0,7} \cdot Pr^{\frac{1}{3}} \cdot A \cdot e^{-(B_{Nu}+C_{Nu}\cdot\cos(\Phi))\cdot\left(\frac{l_{\text{wk}}}{d_{\text{capillary}}}\right)^m} \quad (25)$$

$$A_{\text{Nu}} = -1{,}45 \cdot 10^{-4} \cdot \left(\frac{l_{\text{wk}}}{d_{\text{capillary}}}\right) + 0{,}151 \quad (26)$$

$$\text{B}_{\text{Nu}} = 0{,}18 \cdot \Theta^2 - 0{,}54 \cdot \Theta + 0{,}78 \quad (27)$$

$$C_{\text{Nu}} = 0{,}16 \cdot \Theta^2 - 0{,}67 \cdot \Theta + 0{,}66 \quad (28)$$

Since a 1-phase liquid state is implied for the correlation, the material properties are determined according to the viscosity model. To cause the centrifugal acceleration of the refrigerant, a twisted band was inserted into the cylindrical bushing.

The heat transfer in the 2-phase swirl region is formalized according to a correlation by Yagov, [8]. This is subsumed from the heat flow through bubble boiling and for convective heat transfer in chapter 6.5 of [2].

$$q_{\text{b}} = 3{,}43 \cdot 10^{-4} \cdot \left(\frac{\lambda^2 \cdot \Delta T_{\text{s}}^3}{\nu \cdot \sigma \cdot T_{\text{s}}}\right) \cdot \left(1 + \frac{h_{\text{LG}}}{2 \cdot R_{\text{i}} \cdot T_{\text{s}}^2} \Delta T_{\text{s}}\right) \cdot (1 + \sqrt{1 + 800 \cdot B_{Nu,tp}} + 400 \cdot B_{Nu,tp}) \quad (29)$$

$$B_{\text{Nu,tp}} = \frac{h_{\text{LG}}}{\sigma} \cdot \left(\frac{(\nu \cdot \rho_{\text{G}})^3}{\lambda \cdot T_{\text{s}}}\right)^{0,5} \quad (30)$$

$$\Delta T_{\text{s}} = T_{\text{w}} - T_{\text{s}} \quad (31)$$

According to Yagov [8], the share of heat transfer by bubble boiling only becomes dominant at a heat flow density of $8\,\text{MW/m}^2$ and high mass flow velocities of more than $56.000\,\text{kg/(m}^2 \cdot \text{s)}$ dominant. For this application the heat flux density in the spray area is $13\,\text{kW/m}^2$ and in the swirl area $0{,}1\,\text{MW/m}^2$. The influence of bubble boiling on heat transfer with large differences in the absolute amounts to the convective heat flow fraction is shown by:

$$q = \left(q_{\text{c}}^3 + q_{\text{b}}^3\right)^{\frac{1}{3}} \quad (32)$$

At high mass flow velocity, both heat transfer mechanisms act independently of each other and can be superimposed.

Lopina and Bergles [9] developed an empirical correlation for the 1-phase heat transfer coefficient. Tests were carried out with the fluid water at pipe diameters close to 5 mm. The correlation has the best agreement with test results for heating of liquid fluid [8]. The simulation evaluation uses diameters $D_{\text{Evaporator}}$ between 8 and 14 mm. From this comparison, differences are to be expected in addition to the geometric deviation between the screw and the twisted strip.

The improvement of heat transfer by the swirl flow was formalized by 3 factors in the correlation. Heat flow fraction is shown by:

$$\alpha_{\text{s}} = \frac{\lambda}{D_{\text{hyd}}} \cdot F \cdot \left(0{,}023 \cdot \left(\text{k}_1 \cdot Re_{\text{hyd}}\right)^{0,8} \cdot \text{Pr}^{0,4} + 0{,}193 \cdot \left(\left(\frac{Re_{\text{hyd}}}{y}\right)^2 \frac{D_{\text{hyd}}}{D_{\text{i}}} \cdot \beta \cdot \Delta T \cdot Pr\right)^{\frac{1}{3}}\right) \quad (33)$$

First term of the equation corresponds to a common correlation for convective heat transfer for a smooth straight pipe, consisting of a product of Reynolds and Prandtl number adjusted with the correction factor k_1 due to increase in axial velocity.

$$k_1 = \left(1 + \frac{\pi^2}{4 \cdot y^2}\right)^{0,5} \quad (34)$$

Second term of the equation considers the uneven distribution of density in the eddy current field due to mass forces caused by centrifugal acceleration.

The factor F considers the surface and material properties of the ribs of the twisted strip. Since the swirl evaporator is equipped with a threaded screw, it is not necessary to consider F for this application. For lack of better alternatives to formalize the physics for heat transfer in the swirl range, this correlation was maintained.

The model quantifies the change of state between capillary inlet and swirl outlet, considering pressure losses and heat flux. The program consists of several procedures (subroutines) and a main program to call them. With the implemented correlations of the individual regimes, the simulation calculates the pressure loss with a given starting value for the mass flow and other operating parameters. Pressure loss and heat transfer are determined independently. First, the mass flow is adjusted by a defined step size of 1000 Pa in iterations until a pre-set tolerance deviation between the target evaporation pressure and the simulated evaporation pressure is undershot. Then, the program begins to calculate the heat transfer with the determined mass flow. Adjustments are also necessary for the correlations of heat transfer in the spray, swirl 1-phase and 2-phase regimes. According to a distribution determined from FEM simulations, the defined target heat flow is distributed around 5% to the spray regime and the rest to the swirl. The simulation is deterministic. Starting from an initial value for the mass flow, all correlations for the pressure loss are calculated chronologically along the regimes and at the end of an iteration the deviation from the target evaporation pressure is calculated. Depending on whether the deviation is positive or negative, the mass flow is increased or decreased by one increment. This is repeated until the value falls below a pre-set tolerance deviation. The parameterization Nusselt-correlation for the spray is supplemented by 2 correction factors K_1 and K_2 and has the form

$$Nu_{\text{Spray}} = K_1 \cdot Re_{d_{\text{capillary}}}^{0,7 \cdot P_{\text{r}}^{\frac{1}{3}}} \cdot A_{\text{Nu,spray}} \cdot e^{\left(-\left(B_{\text{Nu,spray}} + C_{\text{Nu,spray}} \cdot \cos(\phi)\right) \cdot \left(\frac{l_{\text{wk}}}{d_{\text{capillary}}}\right)^m\right) - K_2} \quad (35)$$

The correction factor K_2 is static. Only K_1 is changed by

one increment during an iteration until the deviation is less than 1 W. For the parameterization Nusselt-correlation of the swirl part a correction factor K_1 is introduced for the heat transfer in the swirl. It is entered as a factor in:

$$Q_{\text{Swirl}} = K_1 \cdot ({q_{c_{\text{Swirl}}}}^3 + {q_{b_{\text{Swirl}}}}^3)^{\frac{1}{3}} \cdot dA_{\text{Nu,swirl}} \quad (36)$$

For a better overview of the simulation and its correlations a flowchart of the simulation is shown in Fig. 5.

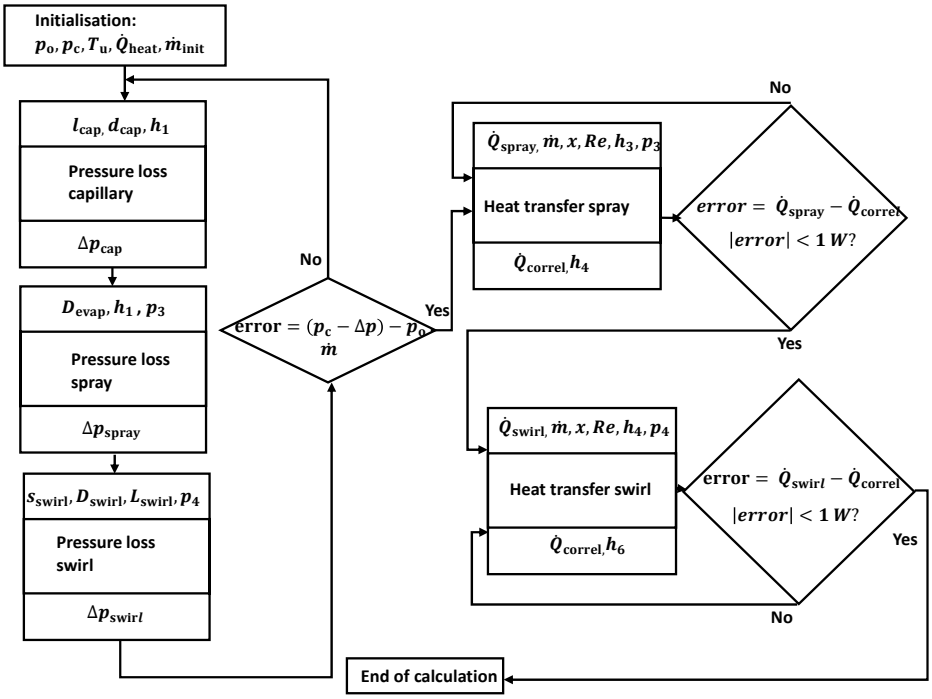

Fig. 5 Flowchart of the simulation

IV. Verification of the Simulation Model

In order to verify the simulation model, the calculated results are compared with the experimental measurements at the test stand described in [10]. As shown in Fig. 6 several penetration depths had been tested and each experiment was at least 3 times in steady state conditions in a controlled and air-conditioned environment.

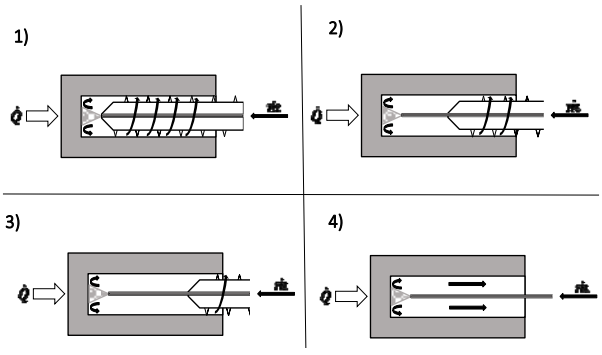

Fig. 6 Various penetration depths of the screw

The measured pressure drop is used to calculate the mass flow of the simulation. Therefore, they also have error bars in both cases of one standard derivation.

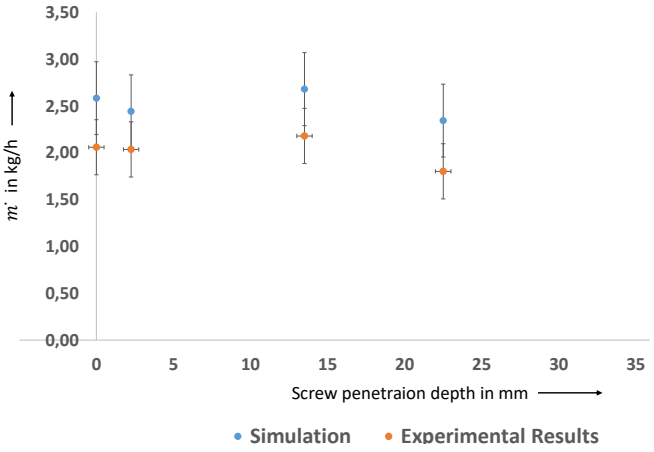

Fig. 7 Comparison of the simulation to the experimental results

The experimental results show overall good correlation with the simulated results. For penetration depths less than 25 mm the simulation seems to overestimate the mass flow and for a penetration depth of 40 mm the simulation is underestimating the measured values.

V. Hydraulic Optimization

The current swirl evaporator uses a screw with a constant step size to generate the vortex flow in the swirl section. The

refrigerant evaporates as it flows through the screw threads and the vapor content increases. Due to the higher quality and lower mixed density the volume flow increases:

$$\dot{V} = \frac{\dot{m}}{\rho} \tag{37}$$

and hence

$$c = \frac{\dot{V}}{A_{\mathrm{hyd}}} \tag{38}$$

Also, the flow velocity increases. In order to optimize the swirl evaporator regarding to pressure loss, the flow velocity should be kept constant which means the cross-sectional area A_{hyd} needs to increase simultaneously.

$$\frac{dV}{dt} \cdot \frac{dz}{dA_{\mathrm{hyd}}} = const. \tag{39}$$

In a discretized model this means

$$c[i] = c[i+1]. \tag{40}$$

or

$$\frac{\dot{V}[i]}{A[i]} = \frac{\dot{V}[i+1]}{A[i+1]}. \tag{41}$$

respectively.

In praxis, this means that the screw with a constant step size as shown in Fig. 8 is changed to a screw with variable step size as shown in Fig. 11 to maintain a constant flow velocity of the refrigerant and therefore minimize pressure loss within the system, which has the additional benefit of minimizing the evaporation temperature drop without the use of azeotrope refrigerants. The optimized screw is shown in Fig. 11.

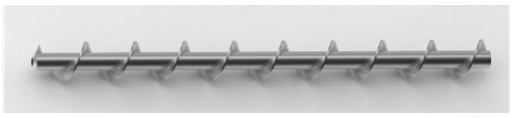

Fig. 8 Screw with constant step

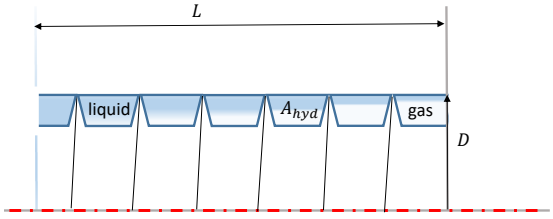

Fig. 9 Sketch of a screw with constant step

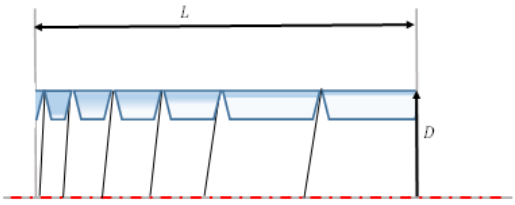

Fig. 10 Sketch of a screw with variable step

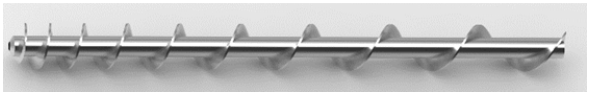

Fig. 11 Screw with variable step

VI. Conclusion

In this paper a model was presented to design a swirl evaporator and to simulate its thermodynamic behavior. The pressure drop in the swirl evaporator is determined with acceptable accuracy of less than one standard derivation of the measured values. A method was presented to design the swirl evaporator specifically for the respective application and minimize pressure loss in the swirl part.

Nomenclature

TABLE I
Variables Used for Calculation of the Swirl Evaporator

Symbol	Quantity	Conversion from Gaussian and CGS EMU to SI
a	thermal diffusivity	m²/s
c	flow velocity	m/s
$d_{\mathrm{capillary}}$	diameter capillary	m
$dA_{\mathrm{Nu,swirl}}$	swirl area	m²
dL	length of the pipe relevant for pressure loss	m
l_{wk}	distance between capillary outlet and cooling wall	m
$\mathrm{k_1}$	correction factor to increase in axial velocity	-
h_{LG}	Evaporation enthalpy of the fluid	kJ/kg
$l_{\mathrm{0,Swirl}}$	length of the flow path	m
m	experimental factor	-
n	number pf revolutions of the swirl	-
p_{krit}	critical pressure of the refrigerant	Pa
q	heat flux	W/m²
q_{b}	heat flux by bubble boiling	W/m²
$q_{\mathrm{b_{Swirl}}}$	heat flux by bubble boiling, swirl	W/m²
q_{c}	heat flux by convective boiling	W/m²
$q_{\mathrm{c_{Swirl}}}$	heat flux by convective boiling, swirl	W/m²
w_{G}	pipe gas velocity	m/s
w_{M}	mean flow velocity	m/s
x	quality	-
y	Pitch at 180° rotation related to the diameter of the screw	-
A	area of the flow cross section	m²
A_{Nu}	correlation factor for the Nusselt-Number-Correlation	-
$\mathrm{A_{Nu,spray}}$	correlation factor for the Nusselt-Number-Correlation, iterative	-
B_{Nu}	correlation factor for the Nusselt-Number	-
$B_{\mathrm{Nu,spray}}$	correlation factor for the Nusselt-Number-Correlation, iterative	-
$B_{\mathrm{Nu,tp}}$	Two-phase factor	-
C_{Nu}	correlation factor for the Nusselt-Number	-
$C_{\mathrm{Nu,spray}}$	correlation factor for the Nusselt-Number-Correlation, iterative	-
D	pipe diameter	m
D_{evap}	diameter evaporator	
D_{hyd}	hydraulic diameter	m
$D_{\mathrm{hyd_{Swirl}}}$	hydraulic diameter swirl	m
D_{i}	inner diameter	m

Symbol	Quantity	Conversion from Gaussian and CGS EMU to SI
F	Surface and material properties factor of the twisted strip	-
G	mass flow density	Kg/(m²·s)
K_1	Correction factor for the heat transfer	-
K_2	Correction factor, iterative calculation	-
Q_{Swirl}	Heat load in the swirl area	W
L	characteristic length of the heat transfer task	m
Pr	Prandtl-number	-
Re	Reynolds number	-
$Re_{\mathrm{d_{capillary}}}$	Reynolds-number for the capillary diameter	-
R_{i}	specific gas constant	J/
T_{s}	temperature of the Swirl flow	K
T_{w}	temperature effective heat transfer surface	K
U	circumference of the flow cross section	m
X_{xp}	mixed quality	-
α	heat transfer	W/(m²·K)
α_{s}	heat transfer coefficient Swirl area	W/(m²·K)
γ_{Spray}	factor for the calculation of the pressure drop of the spray	-
ζ	drag coefficient	-
ζ_{Spray}	drag coefficient spray channel	-
η_{L}	Dynamic viscosity liquid	m·Pa·s
k_{slip}	correlation factor for pressure loss	-
λ	thermal conductivity of a fluid	W/(m·K)
λ_{L}	volume flow portion liquid phase	-
ν	kinematic viscosity	m²/s
ν_{L}	viscosity of a liquid	kg/(m·s)
ν_{tp}	viscosity of a two-phase	kg/(m·s)
ρ_{G}	density of a gas	kg/m³
ρ_{L}	density of liquid phase	kg/m³
ρ_{M}	mixture density	kg/m³
σ_{ar}	area ratio	-
σ	surface tension	N/m
Φ	two-phase multiplier Swirl flow	◦
ψ	Coefficient for two-phase pressure drop calculation	-
Δp_0	difference of the evaporation pressure	Pa
Δp_{tp}	pressure difference two-phase	Pa
$\Delta p_{\mathrm{tp,Spray}}$	pressure difference two-phase spray	Pa
$\Delta p_{\mathrm{tp_{Swirl}}}$	pressure difference two-phase swirl	Pa
ΔT	difference temperature	K
ΔT_{s}	difference temperature effective heat transfer surface to the swirl flow temperature	K
Θ	spray angle in radiant	-

REFERENCES

[1] W. W. Akers, H. A. Deans und O. K. Crosser, Condensing heat transfer within horizontal tubes, 1958
[2] VDI-GVC und VDI e.V., Hrsg., VDI-Wärmeatlas, Heidelberg, 2006.
[3] Mueller, N. und Puerta, G.: Pressure drop sudden enlargement of a pipe, SE5M0003, CSE Institute, Pfinztal, with Chisholm correlations.
[4] G.-d. Xia, „An investigation of two-phase flow pressure drop in helical rectangular channel," ElsevIer, 2014.
[5] L. Chen, „Steam-water two-phase flow frictional pressure drop in straight tubes," 1982.
[6] B. A. Lindeman, J. M. Anderson und T. A. Shedd, „Predictive model for heat transfer performance of oblique and normally," Elsevier, Wisconsin Madison, USA, 2013.
[7] R. J. Goldstein und M. E. Franchett, „Heat transfer from a flat surface to an oblique impinging jet," 1988.
[8] V. V. Yagov, Heat transfer and crisis in swirl flow boiling, Moskau: Elsevier, 2005.
[9] R. F. Lopina und A. E. Bergles, Heat transfer and pressure drop in tape generated swirl flow, 1969.
[10] M. Feiner, M. Kipfmüller, M. Arnemann, Development of an Adjustable Spiral-shaped Evaporator17th International Refrigeration and Air Conditioning Conference at Purdue, 2018
[11] Poiseuille, J. L. M. 1846. Recherches experimentales sur Ie mouvement des liquides dans les tubes de tres-petits diametres, Academie Royale des Sciences de l'Institut de France, IX:
[12] Gnielinski, V.: Ein neues Berechnungsverfahren für die Wärmeübertragung im Übergangsbereich zwischen laminarer und turbulenter Rohrströmung,
[13] Gnielinski, V.: Neue Gleichungen für den Wärme- und den Stoffübergang in turbulent durchströmten Rohren und Kanälen, Forschung im Ingenieurwesen (Engineering Research), 41 (1975) 8-16.
[14] Knipping, T. (2018): Kühlen kleiner Kavitäten mit verdampfenden Fluiden. DKV-Forschungsbericht, No. 88